Opto-Electronic Advances

Original Article

2022, Vol. 5, No. 12

DOI: 10.29026/oea.2022.210081

All-fiber-transmission photometry for simultaneous optogenetic stimulation and multi-color neuronal activity recording

Zhongyang Qi[1,2,3†], Qingchun Guo[4,5,6†], Shu Wang[6], Mingyue Jia[6], Xinwei Gao[6], Minmin Luo[3,6,7*] and Ling Fu[1,2*]

Manipulating and real-time monitoring of neuronal activities with cell-type specificity and precise spatiotemporal resolution during animal behavior are fundamental technologies for exploring the functional connectivity, information transmission, and physiological functions of neural circuits *in vivo*. However, current techniques for optogenetic stimulation and neuronal activity recording mostly operate independently. Here, we report an all-fiber-transmission photometry system for simultaneous optogenetic manipulation and multi-color recording of neuronal activities and the neurotransmitter release in a freely moving animal. We have designed and manufactured a wavelength-independent multi-branch fiber bundle to enable simultaneous optogenetic manipulation and multi-color recording at different wavelengths. Further, we combine a laser of narrow linewidth with the lock-in amplification method to suppress the optogenetic stimulation-induced artifacts and channel crosstalk. We show that the collection efficiency of our system outperforms a traditional epi-fluorescence system. Further, we demonstrate successful recording of dynamic dopamine (DA) responses to unexpected rewards in the nucleus accumbens (NAc) in a freely moving mouse. We also show simultaneous dual-color recording of neuronal Ca^{2+} signals and DA dynamics in the NAc upon delivering an unexpected reward and the simultaneous optogenetic activating at dopaminergic terminals in the same location. Thus, our multi-function fiber photometry system provides a compatible, efficient, and flexible solution for neuroscientists to study neural circuits and neurological diseases.

Keywords: fiber photometry; all-fiber-transmission; multi-color; optogenetic; neuroscience

Qi ZY, Guo QC, Wang S, Jia MY, Gao XW et al. All-fiber-transmission photometry for simultaneous optogenetic stimulation and multi-color neuronal activity recording. *Opto-Electron Adv* **5**, 210081 (2022).

Introduction

The abilities to optogenetically manipulate and monitor neuronal activity with cell-type specificity are indispensable methods for neuroscientists to study neural circuits in behaving animals[1–4]. In particular, heterogeneous populations of neurons and various neurotransmitters[5] comprise neural circuits of different functions, exhibiting distinctive neuronal activities[6] corresponding to specific

[1]Britton Chance Center for Biomedical Photonics, Wuhan National Laboratory for Optoelectronics, Huazhong University of Science and Technology, Wuhan 430074, China; [2]MoE Key Laboratory for Biomedical Photonics, School of Engineering Sciences, Huazhong University of Science and Technology, Wuhan 430074, China; [3]National Institute of Biological Sciences, Beijing 102206, China; [4]Beijing Advanced Innovation Center for Big Data-Based Precision Medicine, Beijing 100191, China; [5]School of Biomedical Engineering, Capital Medical University, Beijing 100069, China; [6]Chinese Institute for Brain Research, Beijing 102206, China; [7]School of Life Sciences, Tsinghua University, Beijing 100084, China.

[†]These authors contributed equally to this work.

*Correspondence: MM Luo, E-mail: luominmin@nibs.ac.cn; L Fu, E-mail: lfu@mail.hust.edu.cn

Received: 1 July 2021; Accepted: 28 September 2021; Published online: 20 May 2022

behaviors[4,7]. For example, dopamine (DA) neurons are known to have two different firing patterns: the phasic pattern and the tonic pattern. These patterns induce distinct activities in their downstream neurons, which are involved in diverse physiological functions[6,8,9]. Moreover, the dentate 'gate' hypothesis of seizures has been experimentally evaluated *in vivo* using a closed-loop system to record and optogenetically manipulate the activity of granule cells during seizures in mice[10]. Thus, simultaneous optogenetic manipulation and multi-color recording to monitor feedback effects resulting from optogenetic circuit interventions are now recognized as the method of dreams for the causal investigations of neural circuits and neurological diseases.

However, previous techniques or systems to optogenetically manipulate or monitor neuronal activity in behaving animals are mostly separated and work independently[11–23]. Few studies have attempted to combine optogenetic manipulation and neuronal activity recording into a single system[24–28]. The optrode, which integrates electrophysiological recording[29] with the optogenetic stimulations[24,30], is the most widely used method to record and manipulate neurons, but it cannot directly monitor neurotransmitter activities. Enabled by the development of genetically encoded fluorescent indicators (GEFI)[31–35], optical imaging technologies including the miniature fluorescence microscope[18,27] and the miniaturized two-photon microscope[17,36] are capable of imaging and manipulating neurons at the same time. By implanting a gradient refractive index (GRIN) lens in the brain, these imaging techniques support direct imaging and optogenetic manipulation of specific types of neurons at single-cell resolution in deep brain regions of freely moving animals[37]. However, an implanted GRIN lens is usually in a diameter of 500 μm to 1 mm, thus inducing substantial damages to the brain[38,39]. Furthermore, the current systems implemented with endoscopic imaging techniques are only capable of optogenetic manipulation and single-channel recording at a single wavelength.

As an alternative technique that induces less invasion, fiber photometry[14,15,25,26,40–42] provides a unique feature for an easy and stable recording of population activities with cell-type specificity in freely moving animals. Various approaches have been proposed to incorporate optogenetics with fiber photometry, enabling wide applications and the discovery of many functional insights[25,26,41]. However, since the excitation spectrum of Channelrhodopsin-2 (ChR2, 473 nm)[1,43] is close to the emission spectrum of the Ca^{2+} indicator Oregon green 488 BAPTA-1 (OGB-1) or GCaMP (both peak at ~510 nm), and considering that it is quite challenging to completely filter out optogenetic stimulation light with milliwatt, obvious artifacts from optogenetic stimulation are inevitable in a weak (pico watt) fluorescent signal during recording (Supplementary information Fig. S1(a))[25]. Replacing ChR2 with a fast red-shifted channelrhodopsin, (e.g., bReaChES, 594 nm) can significantly reduce the artifacts observed with ChR2 (Supplementary information Fig. S1(b))[26]. However, only one type of neuron or neurotransmitter can be monitored in this case, and stimulation artifact is still a problem when involving dual-color recording, as the excitation spectrum of bReaChES overlaps with the emission spectrum of the RFP-based GEFIs (Supplementary information Fig. S1(c)).

To achieve simultaneous optogenetic manipulation and dual-color recording, more wavelength-range fluorescent proteins with spectral spacing (the peak emission wavelength of GEFIs to the effective excitation wavelength of opsin-sensors should exceed ~60 nm, Supplementary information Fig. S1(d)) need to be involved and the optical system is thus required to fully cover the visible spectrum. However, the currently available fiber photometry systems only cover the spectrum of 405~600 nm by using the classical epifluorescence imaging architecture (Supplementary information Fig. S2)[26] consists of an objective lens and two or three dichroic mirrors. In this case, more dichroic mirrors are needed to couple the multiple wavelength light beams into one optical fiber, which makes the system more complex to extend the spectrum. Therefore, to make a compatible and flexible system, an all-fiber-transmission optical system can deliver multiple-wavelength light for simultaneous optogenetics and neuronal activity recording, and collect multi-color fluorescence signals.

Here, we developed an all-fiber-transmission photometry system based on a multi-branch fiber bundle[44–46] for simultaneous optogenetic manipulation and multi-color recording of neuronal Ca^{2+} or neurotransmitter signals in a freely moving animal. Briefly, a non-wavelength selective multi-branch fiber bundle is combined with a PMT to replace the traditional imaging structure. The multi-function fiber photometry system can deliver all of the required light using optical fibers, making the system more robust for use in freely behaving experimental contexts. Notably, we adopted a narrow linewidth laser and used a lock-in amplification method[47,48] to successfully manage issues with optogenetic

stimulation artifacts and channel crosstalk. We show that our system has excellent light transmission performance. Moreover, it can be readily reconfigured for simultaneous multi-color recording of neuronal Ca^{2+} signals and neurotransmitter dynamics and precise optogenetic manipulations in freely moving animals.

Materials and methods

Optical setup

Using a custom-designed bifurcated fiber bundle (AlphaTech), we developed an all-fiber-transmission system for single-channel fiber photometry (Fig. 1). The overall appearance and section image of each branch of the bundle is shown in Fig. 1(a). The bifurcated fiber bundle consists of 3 branches in total: the single-fiber branch i, the collection branch ii, and the common branch iii. All these 83 fibers (branch iii) are hexagonally distributed in the common branch and divided into two branches with 1 (branch i) and 82 (branch ii) fibers in each of them (as Fig. 1(a) sub-image shows). To decrease optical transmission loss, the bundle length was limited to about 350 mm. The structure of common branch iii is shown in Fig. 1(b). The fiber we use in our design is glass optical fiber with 50 μm diameter and 0.54 numerical aperture (NA). To match the currently available 200 μm or 400 μm multi-mode fiber and efficiently collect the returned fluorescence, the diameter of the bundle is designed at approximately 500 μm. The single fiber from branch i for excitation light (blue) transmission is placed in the center of branch iii surrounded by the other 82 fibers (branch ii) for collecting fluorescence signals. Fig. 1(c) is a schematic diagram of the single-channel fiber photometry system we constructed using a bifurcated fiber bundle. Excitation light from a 450-nm LED through the single-fiber branch i is coupled into the multi-mode fiber (200 μm in diameter and 0.37 in NA) connecting to the fiber bundle and the animal. The

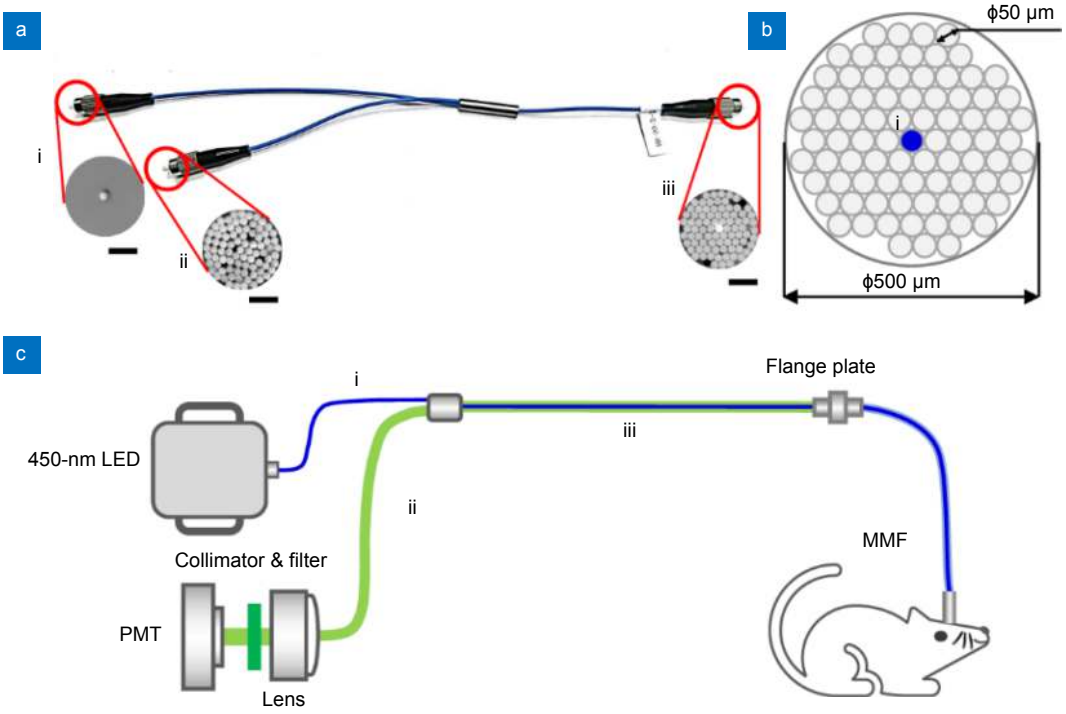

Fig. 1 | A custom-designed bifurcated fiber bundle and all-fiber-transmission single-channel fiber photometry system. (**a**) An image of the bifurcated fiber bundle. The bifurcated fiber bundle consists of 3 branches in total: the single-fiber branch i, the collection branch ii, and the common branch iii. The total length of this bundle is about 350 mm. The sub-image of iii was acquired using a high-intensity excitation light coupled into the single-fiber branch i. Scale bar, 200 μm. (**b**) Diagram of the bifurcated fiber bundle common branch iii. The common branch iii (500 μm) consists of 83 hexagon distributed optical fibers (Φ50 μm/0.54 NA) in total. The single fiber from branch i for excitation light (blue) transmission is placed in the center of branch iii and is surrounded by the other 82 fibers (branch ii) for collecting fluorescence signals. (**c**) Schematic diagram of the all-fiber-transmission single-channel fiber photometry system constructed with a custom-designed bifurcated fiber bundle. The excitation light from an LED is coupled into the multi-mode fiber connected to the animal through the single-fiber branch i. The emission fluorescence is then collected by the common branch iii and delivered to the PMT (behind a collimator and a fluorescence filter). Abbreviations: PMT, photo multiplier tube; MMF, multi-mode fiber. LED, light emitting diode.

emission fluorescence is collected by the common branch and delivered to the PMT (Hamamatsu, H10720-210) behind the collimator (DHC, GCL-010131) and the fluorescence filter (Semrock, FF01-525/39-25).

Using a custom-designed four-branch fiber bundle (AlphaTech), we developed a multi-function fiber photometry system (Fig. 2) that can realize multi-color recording while also supporting precise optogenetic stimulation. Figure 2(a) shows a photo of the bundle consisting of 1 common branch v and 4 splitting branches i–iv. As illustrated in Fig. 2(b), 85 glass optical fibers (50 μm in diameter and 0.54 in NA) are hexagonally distributed in the common branch v. The three brighter fibers in the center of the bundle correspond to the three single-fiber branches i–iii for coupling to three different excitation lights. Considering that the small diameter (50 μm) of the single optical fiber will dramatically reduce the coupling efficiency, a higher power excitation light source is needed to achieve the excitation light intensity of GEFIs (15~40 μW) or opsin (2~20 mW). A schematic diagram of the multi-function fiber photometry system we constructed using this fiber bundle is shown in Fig. 2(c). In this system, we used three light sources with different wavelengths (Source 1：450-nm LED; Source 2：561-nm laser, Changchun New Industries Optoelectronics Technology, MGL-FN-561-100mW; Source 3：660-nm laser, Changchun New Industries Optoelectronics Technology, MRL-III-633-200mW) and coupled them into the multi-mode fiber connecting to the animal using the three single-fiber branches i–iii. 450-nm and 561-nm excitation lights are used to excite the two different GEFIs (450-nm for dopamine sensors and 561-nm for the jGRECO1a Ca^{2+} sensor in this paper) for monitoring neuronal activities, and the 660-nm laser is used for the optogenetic stimulation. The emission fluorescence is then collected by the common branch v and delivered to the PMT (Hamamatsu, H11461-03) behind the collimator (DHC, GCL-010131) and the fluorescence filters (Dual bandpass filter: Chroma, 59012M; 633-nm short-pass filter: Semrock, BSP01-633R-25). The output signals of the PMT are preprocessed by a custom-designed lock-in amplifier (LIA)[47], digitized using a DAQ card (NI, USB-6003), and recorded by a custom LabVIEW script (50 Hz per channel).

As the power of optogenetic stimulation light (2 mW in our experiment) is much higher than the power of excitation light (20~40 μW) for recording, artificial signals may arise during optogenetic stimulation. In our system, we placed a narrow line-width bandpass filter (Thorlabs, FBH660-10) and a short-pass filter (Semrock, BSP01-633R-25) in front of the 660-nm laser and PMT respectively to decrease the stimulation artifacts. Moreover, to separate the fluorescence signals and further inhibit the stimulation artifacts during the dual-color recording and simultaneous optogenetic manipulation, we adopted the lock-in amplification method in our system. As shown in Fig. 2(d), these two excitation lights for recording are modulated by sinusoidal signals with different frequencies (450 nm, 211 Hz; 561 nm, 531 Hz; the modulation frequencies must avoid harmonic interference, eg: powerline harmonics at multiples of 50 Hz)[49,50], and the optogenetic light is often modulated using relatively low frequency (0–50 Hz) square signals. The emission fluorescence signals from the brain are detected by the PMT, and the output signals of the PMT are then de-modulated by the LIA, using the corresponding demodulation signals (211 Hz and 531 Hz sinusoidal signals); the fluorescence signals of different GEFIs can thus be recorded without channel crosstalk and stimulation artifacts.

Lock-in amplifier and data preprocessing

The fluorescence signals are de-modulated from the output signals (f_{PMT}) of the PMT by the LIA, using the corresponding demodulation signals ($f_{\text{ref-green}}$ and $f_{\text{ref-red}}$). As the frequency of the optogenetic stimulation artifact (0~50 Hz) is quite lower than the modulation frequency of these two excitation lights (f_0: 211 Hz; f_1: 531 Hz), the artifact component can be treated as a constant noise (n_{noise}) during the period of stimulation. Thus, the input signal f_{i} (the output signals f_{PMT} of the PMT) can then be represented as:

$$f_{\mathrm{i}} = f_{\mathrm{PMT}} = A\sin(\omega_0 t) + B\sin(\omega_1 t) + n_{\mathrm{noise}} , \quad (1)$$

where A and B are the signal amplitude, and w_0 and w_1 are the angular frequency ($2\pi f_0$ and $2\pi f_1$ respectively).

The corresponding modulation signal $f_{\text{ref-green}}$ and $f_{\text{ref-red}}$ can be set to be:

$$f_{\text{ref-green}} = C\sin(\omega_0 t) , \quad (2)$$

$$f_{\text{ref-red}} = D\sin(\omega_1 t) , \quad (3)$$

where C and D are the amplitude of the corresponding modulation signals.

After the multiplier, the outputs ($f_{\text{c-green}}$ and $f_{\text{c-red}}$) are:

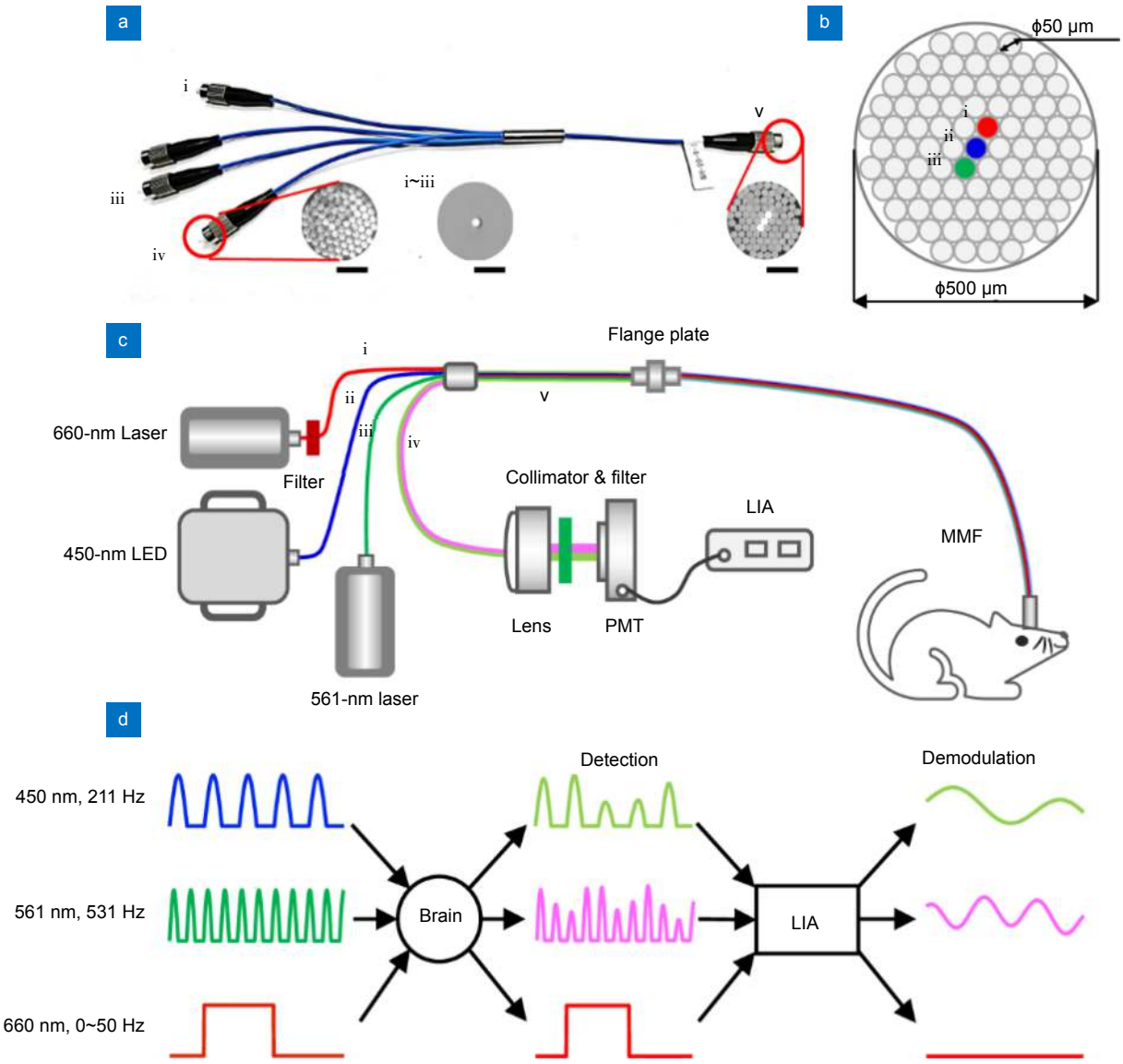

Fig. 2 | A custom-designed four-branch fiber bundle and multi-function fiber photometry system. (**a**) An image of the four-branch fiber bundle. The fiber bundle consists of 5 branches in total: the single-fiber branch i–iii, the collection branch iv, and the common branch v. The total length of this bundle is about 350 mm. The sub-image represents the end face of the single-fiber branch i–iii, the collection branch iv, and common branch v with high-intensity excitation light coupled into the three single-fiber branches i–iii. Scale bar, 200 μm. (**b**) Diagram of the four-branch fiber bundle common branch v. The common branch v (500 μm) consists of 85 hexagon distributed optical fibers (Φ50 μm/0.54 NA) in total. The three brighter fibers in the center of the bundle correspond to the three single-fiber branches i–iii for coupling to three different excitation lights. (**c**) Schematic diagram of the multi-function fiber photometry system constructed with the four-branch fiber bundle. Three light sources with different wavelengths are coupled into the multi-mode fiber and are connected to the mouse through the three single-fiber branches i–iii. The emission fluorescence is then collected by the common branch v and delivered to the PMT (behind the collimator and the fluorescence filters). The output signals of the PMT are preprocessed by a custom-designed lock-in amplifier, digitized using a DAQ card, and recorded using a custom LabVIEW script (50 Hz per channel). (**d**) Schematic diagram of the lock-in amplifier for the multi-function fiber photometry system. These two excitation lights are modulated by sinusoidal signals with different frequencies (450 nm, 211 Hz; 561 nm, 531 Hz). The fluorescent signals can thus be de-modulated from the output signals of the PMT by the LIA, using the corresponding demodulation signals; note that crosstalk does not occur between the green and red channels. The stimulation artifacts caused by the optogenetic light (0~50 Hz) can be further inhibited. Abbreviations: PMT, Photo Multiplier Tube; MMF, Multi-Mode Fiber. LIA, Lock-in amplifier.

$$\begin{aligned} f_{\text{c-green}} =& f_{\text{i}} \times f_{\text{ref-green}} \\ =& (A\sin(\omega_0 t) + B\sin(\omega_1 t) + n_{\text{noise}}) \times C\sin(\omega_0 t) \\ =& \frac{A \times C}{2} - \frac{A \times C}{2}\sin(2\omega_0 t) \\ &+ \frac{B \times C}{2}(\cos((\omega_1 - \omega_0)t) - \cos((\omega_1 + \omega_0)t)) \\ &+ n_{\text{noise}} \times C\sin(\omega_0 t)\ , \end{aligned} \tag{4}$$

$$\begin{aligned} f_{\text{c-red}} =& f_{\text{i}} \times f_{\text{ref-red}} \\ =& (A\sin(\omega_0 t) + B\sin(\omega_1 t) + n_{\text{noise}}) \times D\sin(\omega_1 t) \\ =& \frac{B \times D}{2} - \frac{B \times D}{2}\sin(2\omega_1 t) \\ &+ \frac{A \times D}{2}(\cos((\omega_0 - \omega_1)t) - \cos((\omega_0 + \omega_1)t)) \\ &+ n_{\text{noise}} \times D\sin(\omega_1 t)\ . \end{aligned} \tag{5}$$

According to the Eqs. (4) and (5), when the signals pass through the low-pass filter, the high-frequency components are filtered out, and the fluorescence signals $f_{\text{out-green}}$ and $f_{\text{out-red}}$ can be separated from the mixed fluorescence signals f_{i}:

$$f_{\text{out-green}} = \frac{A \times C}{2}\ , \tag{6}$$

$$f_{\text{out-red}} = \frac{B \times D}{2}\ . \tag{7}$$

Animals

All experiments were approved and were conducted in accordance with the guidelines of the committee on animal health and care of the National Institute of Biological Sciences (NIBS), Beijing.

DAT-Cre mice (JAX Strain 006660) were obtained from the Jackson Laboratory. Male wild-type C57BL6/N mice were purchased from Beijing Vital River Laboratory Animal Technology Co., Ltd (China). All mice were kept under standard conditions of 12/12 hours light-dark cycle (light on 8 PM), with *ad libitum* food and water, except for the sucrose delivery during the fiber photometry experiments, in which mice were deprived of water for 36 hours before the test.

Viral vector preparation

The pAAV-hSyn-GRAB$_{\text{DA2m}}$ plasmid (9.4×10^{12} vg/mL) we used to detect the DA release in NAc was kindly provided by Dr. Yulong Li (Peking University). The AAV-hSyn-Flex-ChrimsonR-mCherry (10^{13} vg/mL) for VTA-NAc terminal stimulation was purchased from Shanghai Taitool Bioscience Co., China. pAAV9-hsyn-NES-jRGECO1a-WPRE (5.06×10^{13} vg/mL) was purchased from Shandong Vigene Biosciences. Inc., China. The AAV-hSyn-EGFP-RPL10 (4.3×10^{12} vg/mL) plasmid in our control experiment was kindly provided by Dr. Fei Zhao (Chinese Institute for Brain Research, Beijing).

Animal surgery and virus injection

Mice were anesthetized by Avertin (i.p., 250 mg/kg) and fixed in a standard stereotaxic frame (RWD Instruments, China). After disinfection with medical alcohol and exposure of the skull, a small craniotomy was made and ~300 nL viruses were delivered using a calibrated pulled-glass pipette (Sutter Instrument); injection into the unilateral targeted brain areas (46 nL/min). All coordinates for the injection sites, as measured from the bregma, include: Nucleus Accumbens core (NAcC): 0.98 mm anterior, 1.3 mm lateral, 4.3 mm ventral; NAc lateral shell (NAcLat): 1.1 mm anterior, 1.3 mm lateral, 4.6 mm ventral; Ventral tegmental area (VTA): 3.4 mm posterior, 0.3 mm lateral, 4.1 mm ventral. After pausing for an additional 5 minutes, the pipette was removed slowly from the brain.

For the fiber photometry and optogenetic experiments, optical fiber (NA: 0.39, diameter: 200 μm; Thorlabs) was implanted 100 μm above the injection site. The ceramic ferrule outside the fiber was then fixed to the skull with super bond C&B dental silicate cement (Parkell Prod). The animals were maintained in their home cage for 2 weeks for recovery and virus expression prior to any testing.

Histology and imaging

After completion of the recording and testing, mice were anesthetized by an overdose of pentobarbital and perfused intracardially with 0.9% phosphate buffer saline and then 4% paraformaldehyde (PFA). The brains were removed carefully and postfixed in 4% PFA for 4 h at room temperature. After cryoprotection in 30% sucrose, coronal sections (50 μm thickness) were cut using a cryostat (Leica, CM1950). The slices were imaged using a slide scanner (Olympus, VS120) with 10x objectives to confirm virus expression and fiber placements. Images were analyzed using ImageJ (NIH).

Data analysis and statistical tests

For fiber photometry recording, the data were acquired by a data acquisition card (National Instrument, USB-6001) and was processed by a custom MATLAB (MathWork, Inc.) program for further analysis. We defined the

value of fluorescence change ($\Delta F/F$) by calculating the following equation:

$$\Delta F/F = (F - F_0)/F_0 , \quad (8)$$

where F_0 is the mean value of the 2 s control time immediately before the behavioral event. The $\Delta F/F$ value was displayed as a heat map or as an average plot (with a shaded area representing the SEM).

For the statistical significance of the event-related fluorescence (ERF) change analysis[3] (Statistically evaluate the degree of correlation between neuronal activity and event stimulation), we performed Wilcoxon signed-rank tests to test the significance of neuronal responses by comparing the $\Delta F/F$ value at each time point with the baseline values (the mean $\Delta F/F$ value of the 2 s control time immediately before the behavioral event). The P-value of each time was superimposed on the average ERF curve with orange lines, indicating a statistically significant (P<0.05) increase.

Results and discussion

Evaluation of the light transmission performance of the all-fiber-transmission photometry system.

In the all-fiber-transmission photometry system, a multi-channel fiber bundle was designed and manufactured to realize the all-fiber transmission of both the excitation light and the emission light. The spectral transmittance of the multi-channel bundle was about 60% per meter in the range of 400 to 900 nm. To decrease optical transmission loss, the bundle length was limited to about 350 mm, thus about 84% of the light was effectively transmitted.

When using the common branch to collect the fluorescence from the multi-mode fiber, part of the fluorescence is guided back to the light source through the single fiber branch, therefore cannot be detected by the PMT. To characterize the loss in fluorescence signal, we tested the collection efficiency of these two systems using a series of sodium fluorescein solutions with different concentrations and compared the results to those acquired using the traditional epi-fluorescence system used in our previous study[3]. We used the same laser, PMT, multi-mode fiber, emission filter, and sodium fluorescein solution in the testing with various systems.

Under the same excitation intensity (40 μW), we tested five concentrations (10~50 ng/mL) and calculated the intensity variation (ΔF) by subtracting the value obtained with pure water. As shown in Fig. 3, our system was linearly correlated with the traditional setup: the red lines represent the fitting curves for the single-channel fiber photometry system (Fig. 3(a), $f(x)$ = 1.297x, R-square: 0.9938) and the multi-function fiber photometry system (Fig. 3(b), $f(x)$ = 1.233x, R-square: 0.9982). The slopes of the fitting curve are 1.297 and 1.233, indicating that the fluorescence collection efficiency of our method was 20–30% better than the traditional setup. These results demonstrated that our all-fiber transmission fiber photometry system based on a multi-branch fiber bundle was capable of effectively exciting and collecting fluorescence signals.

We then evaluated the potential crosstalk between two channels. As shown in Fig. 3(c), we measured the fluorescence intensity of each channel while opening ("on") and closing ("off") the 450-nm and 561-nm excitation lights. We observed no significant change in both channels when the other excitation light was "on" or "off", which demonstrated that no substantial channel crosstalk existed in our all-fiber-transmission photometry system.

We further evaluated the potential stimulation artifacts by measuring the fluorescence intensity of the two channels without the 450-nm and 561-nm excitation light. We observed that the fluorescence intensity of both channels exhibited no response to the optogenetic stimulation (Fig. 3(d)). This demonstrated that the stimulation artifacts can be inhibited to a basal noise level in our all-fiber-transmission photometry system.

Real-time recording of neurotransmitter dynamics in the deep brain region of a freely moving mouse

We then tested the performance of our single-channel fiber photometry system based on a bifurcated fiber bundle by recording DA dynamics at a 100 Hz sampling rate in the nucleus accumbens core (NAcC) of a freely moving mouse. DA is an important neurotransmitter in the brain that exerts functions related to reward, motivation, and motor control[8,51]. The dysfunctions of the DA system are associated with neurological disorders such as Parkinson's disease and schizophrenia[52]. The NAc is known to be a major brain area that accepts DA released from the ventral tegmental area (VTA) DA neurons[53].

We used the single-channel fiber photometry system shown in Fig. 1(c) to monitor DA dynamics when delivering a sucrose solution (12.5 μL, 5% w/v) to a 36-hour water-deprived mouse through a cheek fistula (Fig. 4(a)). The genetically encoded GPCR-activation-based-DA

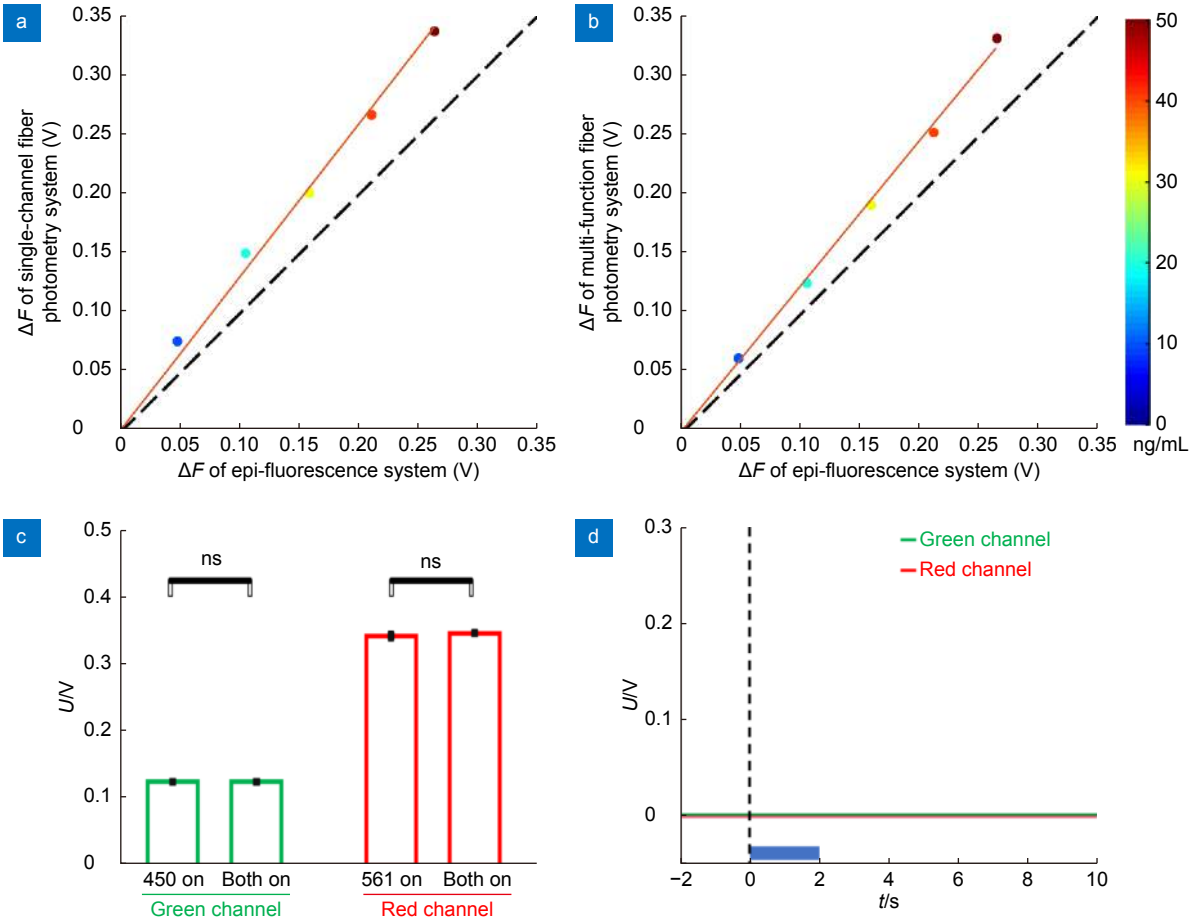

Fig. 3 | Evaluation of the light transmission performance of the all-fiber-transmission photometry system. (**a**, **b**) The fitting curve of the fluorescence intensity variation of a traditional epi-fluorescence system with the all-fiber-transmission photometry system based on the bifurcated fiber bundle (a) or the four-branch fiber bundle (b). The dashed line represents the curve for $y = x$. The red line represents the fitting curve for the single-channel fiber photometry system ($f(x) = 1.297x$, R-square: 0.9938) and the multi-function fiber photometry system ($f(x) = 1.233x$, R-square: 0.9982). (**c**) The mean fluorescence intensity of the green (450 on: 0.1254 ± 0.0003; both on: 0.1257 ± 0.0004) and red (561 on: 0.3421 ± 0.0069; both on: 0.3456 ± 0.0059) channel between the other excitation light "off" and "on". $P>0.05$, Wilcoxon's signed-rank test; $n = 7$ pairs. (**d**) No significant stimulation artifacts are detected in the green and red channels of the all-fiber-transmission photometry system when applying a 660-nm laser stimulation ($P>0.05$, Wilcoxon's signed-rank test; $n = 10$ pairs). The blue bar indicates the time of stimulation.

sensor ($GRAB_{DA2m}$)[33] was expressed in NAcC neurons to monitor the DA release from DA neurons in the VTA in a wild-type mouse. An optical fiber was implanted 100 μm above the injection site for both the delivery of excitation lights and the collection of emitted light. Histology confirmed the locations of the fiber and $GRAB_{DA2m}$ expression in the NAcC two weeks later (Fig. 4(b)).

We measured DA signals in a freely moving mouse upon a 1 s unexpected sucrose solution that was delivered at random inter-trial intervals of 15–25 s (Fig. 4(c)). As shown in Fig. 4(d, e) (Supplementary information Fig. S3), the DA fluorescence signals, excited by 40 μW of 450-nm LED light, significantly increased immediately following the delivery of the unexpected reward ($\Delta F/F = 11.5 \pm 0.9\%$, mean ± SEM; $P<0.05$, Wilcoxon's signed-rank test; $n = 20$ trials with one mouse). It indicated that the dynamics of DA release from the VTA-NAc DA neurons were positively correlated with the reward, consistent with previous studies[33,53]. These results together demonstrated that our all-fiber transmission fiber photometry system can effectively detect temporal fluorescence dynamics and can be used for real-time monitoring of neurotransmitter dynamics in freely moving animals.

Simultaneous recording of neurotransmitter dynamics and neuronal Ca^{2+} signals in the deep brain region of a freely moving mouse

We then tested the performance of a multi-channel fiber photometry system based on a four-branch fiber bundle

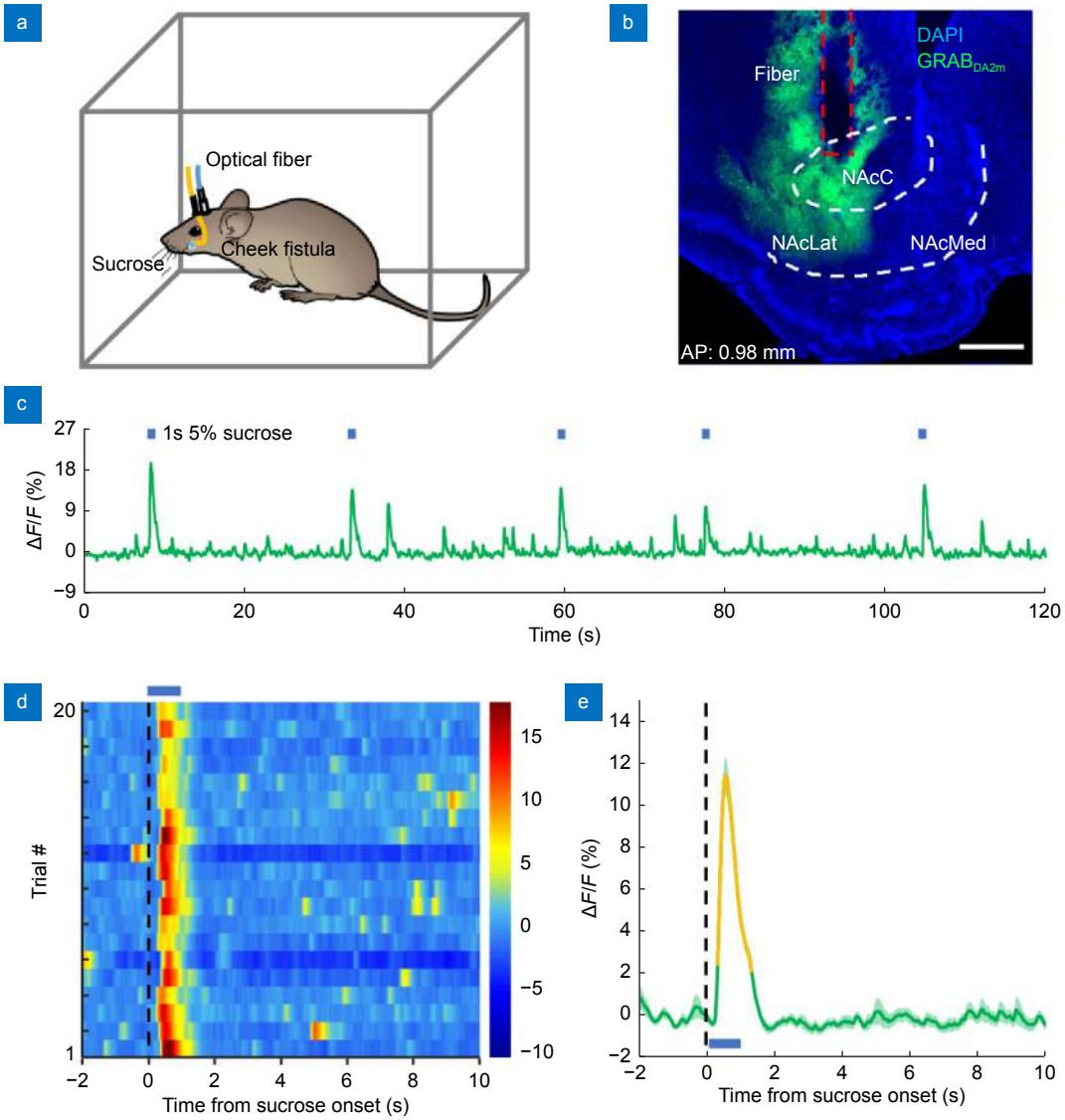

Fig. 4 | Real-time recording of DA dynamics in the NAcC of a freely moving mouse. (**a**) Schematic diagram of the setup for real-time recording of DA dynamics responses to intra-oral 5% sucrose solution delivery through a cheek fistula[3]. The sucrose solution was randomly infused for 20 trials in one behavioral session. (**b**) Histology confirming GRAB$_{DA2m}$ expression (green) in the NAcC brain region. GRAB$_{DA2m}$: Ex 450 nm, Em 525 nm. The brain slice is 0.98 mm anterior to the bregma. Scale bar 500 μm. (**c**) Representative trace of DA signals (encompassing five sequential trials) during the sucrose delivery experiment. The onset times of 5% sucrose solution delivery are indicated above the trace with blue bars. (**d**) Heatmap of DA signal transients aligned to the onset time of sucrose solution delivery. Each row in the heatmap indicates the data for one behavioral trial; 20 trials are plotted. (**e**) Averaged DA signal transients in response to sucrose solution delivery. The shaded area represents ±SEM. The blue bar represents a 1 s sucrose delivery event. Orange segments indicate a statistically significant increase from the baseline (*P<0.05, Wilcoxon's signed-rank test; n = 10 pairs, one mouse). Abbreviations: DA, dopamine; NAc, nucleus accumbens; NAcC, nucleus accumbens core; NAcLat, nucleus accumbens lateral shell; NAcMed, nucleus accumbens medial shell.

by simultaneously recording DA dynamics and neuronal Ca^{2+} signals in the NAc lateral shell (NAcLat). Multiple neuron types that release different neurotransmitters can show various activities in response to a specific function in the NAc or other nucleus; thus, the ability to simultaneously record neuronal activities labeled by multiple-color was essential to study the interactions amongst distinct neuron types in behaving animals[54]. The DA sensor GRAB$_{DA2m}$ (450-nm excitation) and the red Ca^{2+} indicator jGRECO1a (561-nm excitation)[32] were co-expressed in the NAcLat of a wild-type mouse (Fig. 5(a)), and the excitation lights (20 μW) were delivered to the brain through the same optical fiber. Histology confirmed the locations of the fiber and the expression of both GRAB$_{DA2m}$ and jGRECO1a in the NAcLat two weeks later (Fig. 5(b)).

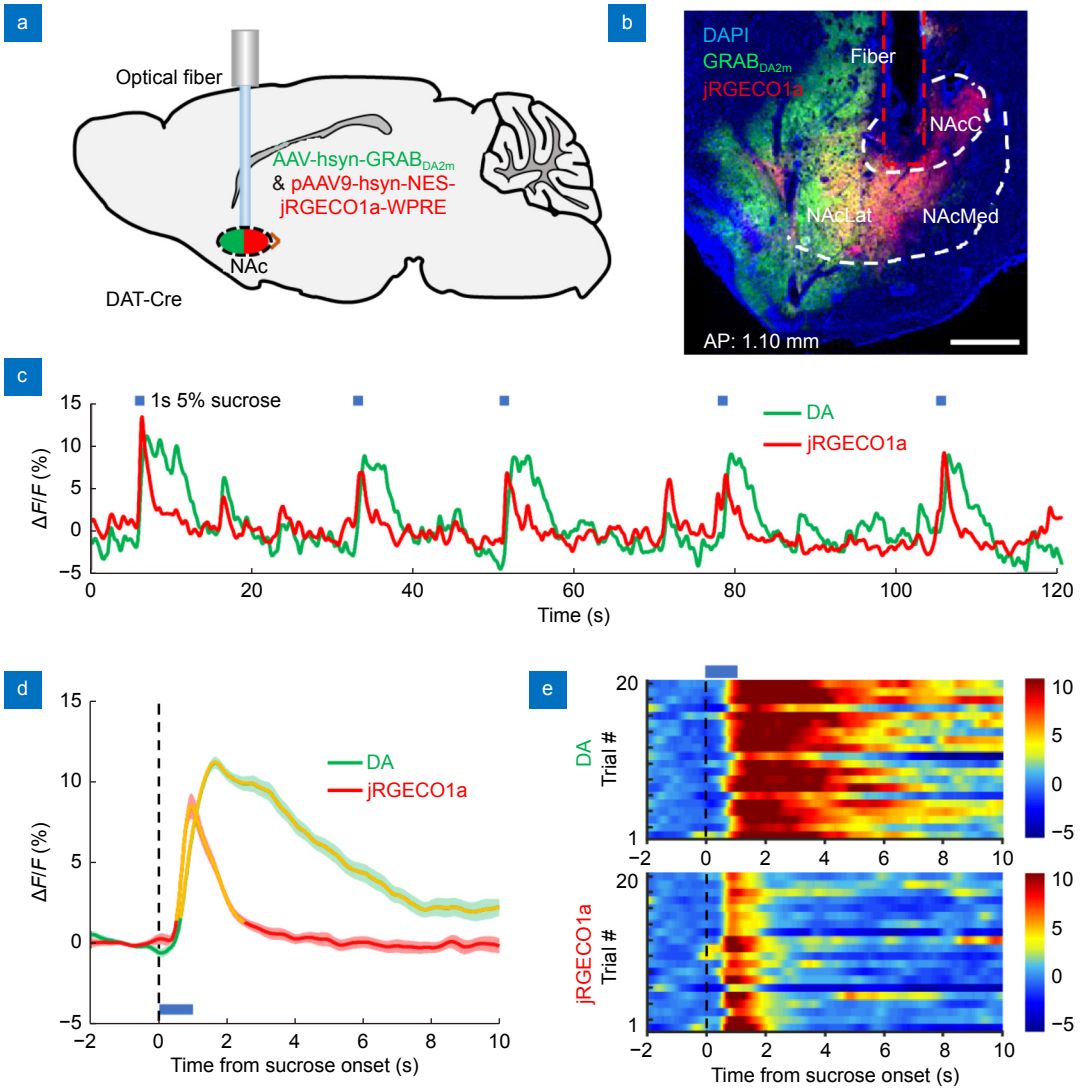

Fig. 5 | Simultaneous recording of dopamine dynamics and neuronal Ca^{2+} signals in the NAcLat of a freely moving mouse. (**a**) Schematic diagram of dual-color recording surgery: we simultaneously record the DA signals (GRAB$_{DA2m}$, green) and the neuronal activity (jGRECO1a, red) in response to a 1 s unexpected sucrose solution in the NAcLat of a freely moving mouse. (**b**) Histology confirming GRAB$_{DA2m}$ (green) and jRGECO1a (red) co-expression in the NAcLat (GRAB$_{DA2m}$: Ex 450 nm, Em 525 nm; jGRECO1a: Ex 561 nm, Em 590 nm). The brain slice is 1.1 mm anterior to the bregma. Scale bar, 500 μm. (**c**) Representative trace of DA signals and neuronal Ca^{2+} signals simultaneously acquired (encompassing five sequential trials) during the sucrose delivery experiment. The onset times of 5% sucrose solution delivery are indicated above the trace with blue bars. (**d**) Averaged DA signal and neuronal Ca^{2+} signal transients in response to unexpected sucrose solution. The shaded area represents the SEM (±). The blue bar represents the 1 s sucrose solution. Orange segments indicate a statistically significant increase from the baseline (*P<0.05, Wilcoxon's signed-rank test; n = 20 pairs, one mouse). (**e**) Heatmap of DA signal and neuronal Ca^{2+} signal transients, aligned to the onset time of sucrose solution delivery. Each row in the heatmap indicates the data for one behavioral trial; 20 trials are plotted. The blue bar represents the delivery of a 1 s sucrose solution. Abbreviations: DA, dopamine; NAc, nucleus accumbens; NAcC, nucleus accumbens core; NAcLat, nucleus accumbens lateral shell; NAcMed, nucleus accumbens medial shell.

We recorded the DA signals and neuronal activities in response to unexpected rewards in a freely moving mouse following the same protocol as described above (Fig. 5(c)). As shown in Fig. 5(d, e), we observed that DA fluorescence signals and neuronal Ca^{2+} signals both significantly increased upon the delivery of unexpected sucrose solutions (DA: $\Delta F/F$ = 11.2 ± 0.4%, jGRECO1a: $\Delta F/F$ = 8.5 ± 0.8%, mean ± SEM; P<0.05, Wilcoxon's signed-rank test; n = 20 trials with one mouse). It indicated that NAcLat neurons and the VTA-NAc DA neurons were positively correlated with the rewards, consistent with previous studies[33,34,53]. However, we noted that these activities had a clear difference in the time course[3] for unexpected rewards (Supplementary information

Fig. 4). Throughout the recording session, the DA signals were correlated with, yet lagged behind, the neuronal Ca^{2+} signals (DA: peak time = 1.91 ± 0.14 s, median latency to peak = 0.99 ± 0.14 s; jGRECO1a: peak time = 0.96 ± 0.02 s, median latency to peak = 0.34 ± 0.04 s, mean ± SEM). Further, the DA signals displayed an overall prolongment of activation (DA: decay duration = 3.81 ± 0.16 s; jGRECO1a: decay duration = 1.08 ± 0.04 s, mean ± SEM). Given that $GRAB_{DA2m}$ and jGRECO1a exhibited similarly rapid rising times[32,33], the result thus suggested that NAc neurons received reward signals from two separate sources: a yet-to-identified input triggered the earlier Ca^{2+} increase, and another input likely from the VTA triggered the slightly later DA release. Together, the results showed strong evidence of heterogeneous neuronal activities in local neuronal circuits. These results also demonstrated that our all-fiber transmission fiber photometry system based on the four-branch fiber bundle can simultaneously detect dynamic fluorescence signals from different GEFIs and was suitable for real-time monitoring of multiple, distinct neuronal activities in freely moving animals.

Simultaneous dual-color recording and optogenetic manipulation of neuronal activities in the deep brain region of a freely moving mouse

We then tested the performance of our multi-function fiber photometry system for simultaneous dual-color recording and precise optogenetic manipulation of neuronal activity in the NAc of a freely moving mouse. Many studies have demonstrated the power of combining simultaneous recording of cell-type-specific neurons and precise optogenetic manipulation of specific neuron types during animal behavior for studies of functional connectivity, activity dynamics, causation between neuronal activities and behaviors, and the physiological functions of neural circuits[4,25,54,55].

VTA dopaminergic neurons are known to project to the NAc and to regulate a variety of physiological processes, including reward, motivation, and motor control[48,56]. We first verified that our system does not elicit stimulation artifacts when simultaneously performing optogenetic manipulation and real-time dual-color recording *in vivo*. A schematic diagram of the experiment is shown in Fig. 6(a): we specifically labeled the VTA DA neurons in a DAT-Cre mouse using a DIO-ChrimsonR-mCherry AAV vector and expressed GFP in all NAcLat neurons. Histology conducted two weeks later confirmed the location of the fiber, the expression of GFP in the somata of NAcLat neurons, and the expression of mCherry in the VTA-NAc dopaminergic terminals (Fig. 6(b)). No significant fluorescence changes were observed in the GFP or mCherry channels during optogenetic stimulation (2 mW, 20 ms per pulse, and 20 Hz for 1 s) (Fig. 6(c), $P>0.05$, Wilcoxon's signed-rank test; n = 10 trials with one mouse), supporting that no obvious stimulation artifacts occurred with our system in this experiment.

Finally, we recorded neuronal Ca^{2+} signals and DA dynamics simultaneously while activating the VTA-NAC dopaminergic terminals in a freely moving mouse. We specifically labeled the VTA DA neurons in a DAT-Cre mouse using a DIO-ChrimsonR-mCherry virus, and co-expressed the DA sensor $GRAB_{DA2m}$ and the red Ca^{2+} indicator jGRECO1a in NAcLat neurons. We recorded the DA signals and jRGECO1a fluorescence signals in a freely moving mouse (50 Hz per channel). As we know, DA neurons exhibit two different firing patterns to induce distinct activities in their downstream neurons and involve diverse physiological functions[6,8]. Then, two different patterns of light pulse stimulations were delivered to the VTA-NAC dopaminergic terminals to induce tonic or phasic firing patterns[48]. We observed that optogenetic phasic stimulation (20-ms per pulse and 20 Hz for 1 s) evoked a significant, time-locked rising trend in the DA signals (DA: $\Delta F/F$ = 6.3 ± 0.7%, mean ± SEM; $P<0.05$, Wilcoxon's signed-rank test; n = 10 trials with one mouse), consistent with a previous study[33]. However, we noted that neuronal Ca^{2+} signals displayed only a slight rising trend (Fig. 6(e), Supplementary. Fig. 5). Upon applying the tonic stimulation (10-ms per pulse and 4 Hz for 5 s), there were no significant changes in either the DA signals or the neuronal Ca^{2+} signals (Fig. 6(f), $P>0.05$, Wilcoxon's signed-rank test; n = 10 trials with one mouse).

These results support previous findings that dopamine is acutely released in the NAcLat when evoked by a burst stimulation of the VTA-NAC dopaminergic terminals[48,57], and suggest that Ca^{2+} signals from population activity are not sensitive to DA release from the VTA neurons in the NAcLat. Notably, to our understanding, such results could not be obtained using conventional electrophysiological recordings: it cannot directly monitor the level of neurotransmitter release[58]. These results support that our system can perform simultaneous

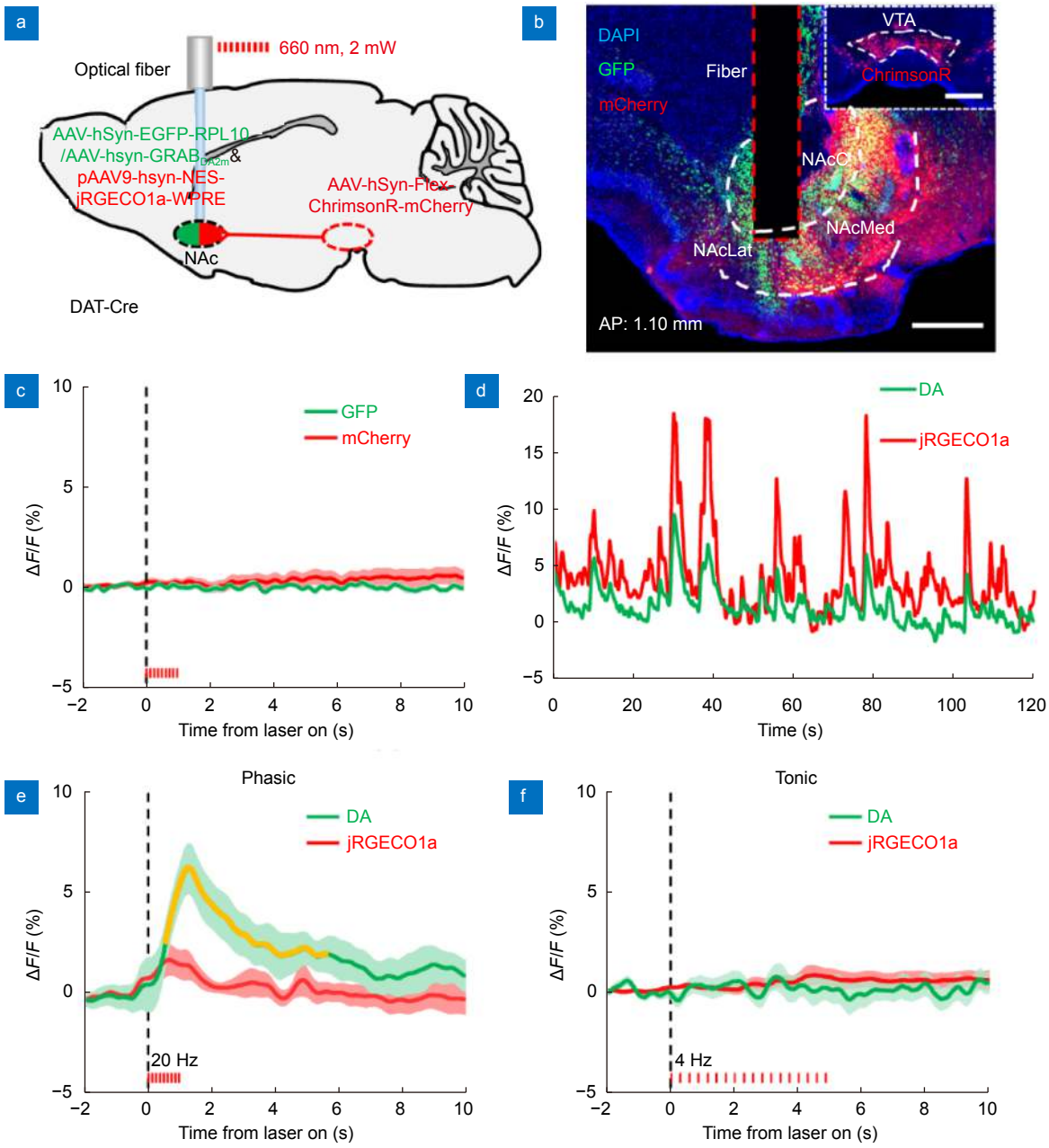

Fig. 6 | Simultaneous dual-color recording and optogenetic manipulation of neuronal activities in the NAcLat of a freely moving mouse. (**a**) Schematic diagram of simultaneous dual-color recording and optogenetic manipulation of neuronal activity surgery: we record GFP and mCherry fluorescence simultaneously, while specifically activating the terminals of VTA-NAc dopaminergic neurons (ChrimsonR: Ex 660 nm) in the NAcLat of a freely moving mouse. Note that GFP was replaced with $GRAB_{DA2m}$ and jGRECO1a in subsequent experiments. (**b**) Histology confirming GFP (green) labeled neurons and ChrimsonR (red) labeled dopaminergic neuron terminal expression in the NAcLat. The brain slice is 1.1 mm anterior to the bregma. Scale bar, 500 μm. (**c**) No stimulation artifacts exist when simultaneously performing optogenetic manipulation and real-time dual-color recording in this system. The red bar indicates the time of stimulation. (P>0.05, Wilcoxon's signed-rank test; n = 20 pairs, one mouse). (**d**) Example of DA and neuronal Ca^{2+}traces simultaneously recorded in the NAcLat of a freely moving mouse. (**e**) Averaged DA signal and neuronal Ca^{2+} signal transients in response to phasic optogenetic stimulation (10 trials). The red bar indicates the time of stimulation. The pulse duration is set to 20 ms at 20 Hz, and lasts for 1 s in each trial. Orange segments indicate a statistically significant increase from the baseline (*P<0.05, Wilcoxon's signed-rank test; n = 10 pairs, one mouse). (**f**) Averaged DA signal and neuronal Ca^{2+} signal transients in response to tonic optogenetic. The red bar indicates the time of stimulation. The pulse duration is set to 10 ms at 4 Hz, and lasts for 5 s in each trial. No significant fluorescence changes are detected in the DA signals or the neuronal Ca^{2+} signals. (P>0.05, Wilcoxon's signed-rank test; n = 10 pairs, one mouse). Abbreviations: DA, dopamine; NAc, nucleus accumbens; NAcC, nucleus accumbens core; NAcLat, nucleus accumbens lateral shell; NAcMed, nucleus accumbens medial shell.

dual-color recording of various neuronal populations while also enabling precise optogenetic manipulation; these combined capacities seem likely to make our system useful for diverse neuroscience functional investigations of various neuron populations and circuits.

Conclusions

We developed a flexible all-fiber transmission fiber photometry system that supports simultaneous dual-color recording of neuronal or neurotransmitter activities combined with precise optogenetic manipulation in freely moving animals. In this system, we designed and manufactured a non-wavelength selective multi-branch fiber bundle to realize the all-fiber transmission of both the excitation light and the emission light, which simplified the system and increased its robustness in freely moving animal experiments. Adopting a laser of narrow line-width for the stimulation and a lock-in amplification method, our system can extract fluorescence signals of two different colors (GFP-based and RFP-based GEFIs) while inhibiting the potential artifacts caused by the optogenetic manipulation (channelrhodopsin with far red-shifted excitation spectrum, 660 nm). Importantly, we showed that our system's collection efficiency was better than a conventional epi-fluorescence system, and we successfully recorded DA dynamics in the NAc of a freely moving mouse. Finally, we successfully recorded both neuronal Ca^{2+} and neurotransmitter dynamic signals in the NAc while also applying precise optogenetic manipulation of the dopaminergic terminals in the same site in a freely moving mouse.

Optogenetic manipulation and monitoring of neuronal activity in a freely moving animal are essential methods for rodent-based neuroscience investigations of brain connectivity and function[1,2]. Several previous studies[24–27] have attempted to combine these two methods to achieve real-time feedback after applying optogenetic stimulation to directly test whether inferred models of dynamics, connectivity, and causation are accurate *in vivo*[4]. However, these methods—including the optrode[24], the miniature fluorescent miniscope[27], the miniaturized two-photon microscope[17], and fiber photometry[25,26,41]—only support the monitoring of one type of neuronal activity when applying optogenetic manipulation at present. A major reason for this is that the action spectrums of the commonly used opsin-sensors[43] like ChR2 (470 nm), eArch3.0 (566 nm), and ChrimsonR (590 nm) are relatively limited, which either have spectral overlap to the excitation spectrum or are too close to the emission spectrum of GEFIs[31,32] like GCaMP6 (510 nm) and jRGECO1a (588 nm). Therefore, when using both the GFP-based and RFP-based GEFIs to label the neurons simultaneously, it is very challenging to completely filter out high-power stimulation light (2~20 mW). And the residual optogenetic stimulation light detected by the detector will lead to obvious artifacts in the acquired signals[4,25,26,41]. Fluorescent proteins with more spectral spacing need to be involved and the optical system is required to fully cover the visible spectrum.

Our design adopted the strategy of all-fiber-transmission by using a small multi-branch fiber bundle to replace the dichroic mirrors and an objective lens, which realized —in a single fiber bundle —three excitation or stimulation lights and two emission lights. In this way, we dramatically simplified the multichannel system and made it more robust and flexible for use in freely behaving experimental contexts. We adopted a laser of narrow line-width of 660-nm to activate the red light–drivable channelrhodopsin (ChrimsonR), therefore inhibited the stimulation-induced artifacts using a lock-in amplification method, which also allowed us to separate the fluorescence signals of the dual-color channels. Our system can be easily modified into different variants for other fluorescent probes and opsin-based sensors by changing the light sources and filter positions before the PMT without adjusting the optical path.

With rapid developments of fluorescent indicators[31,32], such as neurotransmitter probes[33,34,54], light-activated conversion technologies[59,60], a multi-function system is required for neuroscience research[4,10]. Our all-fiber-transmission photometry system supports simultaneous dual-color recording of neuronal or neurotransmitter activities simultaneously with precise optogenetic manipulation in freely moving animals. Thus, it is especially well-suited for the study of interactions amongst different neuron types or neurotransmitters in behaving animals for multiple processes, such as reward[34] or sleep homeostasis[54]. More importantly, our system has the potential to be modified into a closed-loop system that can guide optogenetic manipulation informed by real-time monitoring feedback effects[4,10,25]. The all-fiber-transmission photometry system should be a valuable tool for neuroscientists seeking to comprehensively profile neural circuit functions[3,53,54] and to study neurological diseases[10].

References

1. Boyden ES, Zhang F, Bamberg E, Nagel G, Deisseroth K. Millisecond-timescale, genetically targeted optical control of neural activity. *Nat Neurosci* **8**, 1263–1268 (2005).
2. Grienberger C, Konnerth A. Imaging calcium in neurons. *Neuron* **73**, 862–885 (2012).
3. Li Y, Zhong WX, Wang DQ, Feng QR, Liu ZX et al. Serotonin neurons in the dorsal raphe nucleus encode reward signals. *Nat Commun* **7**, 10503 (2016).
4. Grosenick L, Marshel JH, Deisseroth K. Closed-loop and activity-guided optogenetic control. *Neuron* **86**, 106–139 (2015).
5. Harris JA, Mihalas S, Hirokawa KE, Whitesell JD, Choi H et al. Hierarchical organization of cortical and thalamic connectivity. *Nature* **575**, 195–202 (2019).
6. Chaudhury D, Walsh JJ, Friedman AK, Juarez B, Ku SM et al. Rapid regulation of depression-related behaviours by control of midbrain dopamine neurons. *Nature* **493**, 532–536 (2013).
7. Wang L, Chen IZ, Lin DY. Collateral pathways from the ventromedial hypothalamus mediate defensive behaviors. *Neuron* **85**, 1344–1358 (2015).
8. Tsai HC, Zhang F, Adamantidis A, Stuber GD, Bonci A et al. Phasic firing in dopaminergic neurons is sufficient for behavioral conditioning. *Science* **324**, 1080–1084 (2009).
9. Floresco SB, West AR, Ash B, Moore H, Grace AA. Afferent modulation of dopamine neuron firing differentially regulates tonic and phasic dopamine transmission. *Nat Neurosci* **6**, 968–973 (2003).
10. Krook-Magnuson E, Armstrong C, Bui A, Lew S, Oijala M et al. *In vivo* evaluation of the dentate gate theory in epilepsy. *J Physiol* **593**, 2379–2388 (2015).
11. Adelsberger H, Grienberger C, Stroh A, Konnerth A. In vivo calcium recordings and channelrhodopsin-2 activation through an optical fiber. *Cold Spring Harb Protoc* **2014**, pdb.prot084145 (2014).
12. Liu ZX, Zhou JF, Li Y, Hu F, Lu Y et al. Dorsal raphe neurons signal reward through 5-HT and glutamate. *Neuron* **81**, 1360–1374 (2014).
13. Zhao HX, Li K, Yang F, Zhou WH, Chen NB et al. Customized anterior segment photoacoustic imaging for ophthalmic burn evaluation *in vivo*. *Opto-Electron Adv* **4**, 200017 (2021).
14. Adelsberger H, Garaschuk O, Konnerth A. Cortical calcium waves in resting newborn mice. *Nat Neurosci* **8**, 988–990 (2005).
15. Guo QC, Zhou JF, Feng QR, Lin R, Gong H et al. Multi-channel fiber photometry for population neuronal activity recording. *Biomed Opt Express* **6**, 3919–3931 (2015).
16. Stosiek C, Garaschuk O, Holthoff K, Konnerth A. *In vivo* two-photon calcium imaging of neuronal networks. *Proc Natl Acad Sci USA* **100**, 7319–7324 (2003).
17. Zong WJ, Wu RL, Li ML, Hu YH, Li YJ et al. Fast high-resolution miniature two-photon microscopy for brain imaging in freely behaving mice. *Nat Methods* **14**, 713–719 (2017).
18. Ghosh KK, Burns LD, Cocker ED, Nimmerjahn A, Ziv Y et al. Miniaturized integration of a fluorescence microscope. *Nat Methods* **8**, 871–878 (2011).
19. Cui GH, Jun SB, Jin X, Pham MD, Vogel SS et al. Concurrent activation of striatal direct and indirect pathways during action initiation. *Nature* **494**, 238–242 (2013).
20. Cui GH, Jun SB, Jin X, Luo GX, Pham MD et al. Deep brain optical measurements of cell type-specific neural activity in behaving mice. *Nat Protoc* **9**, 1213–1228 (2014).
21. Li L, Tang YJ, Sun LQ, Rahman K, Huang K et al. *In vivo* fiber photometry of neural activity in response to optogenetically manipulated inputs in freely moving mice. *J Innovative Opt Health Sci* **10**, 1743001 (2017).
22. Guo J, Ran MZ, Gao ZL, Zhang XX, Wang D et al. Cell-type-specific imaging of neurotransmission reveals a disrupted excitatory-inhibitory cortical network in isoflurane anaesthesia. *eBioMedicine* **65**, 103272 (2021).
23. Guan BO, Jin L, Ma J, Liang YZ, Bai X. Flexible fiber-laser ultrasound sensor for multiscale photoacoustic imaging. *Opto-Electron Adv* **4**, 200081 (2021).
24. Anikeeva P, Andalman AS, Witten I, Warden M, Goshen I et al. Optetrode: a multichannel readout for optogenetic control in freely moving mice. *Nat Neurosci* **15**, 163–170 (2012).
25. Stroh A, Adelsberger H, Groh A, Rühlmann C, Fischer S et al. Making waves: initiation and propagation of corticothalamic Ca^{2+} waves in vivo. *Neuron* **77**, 1136–1150 (2013).
26. Kim CK, Yang SJ, Pichamoorthy N, Young NP, Kauvar I et al. Simultaneous fast measurement of circuit dynamics at multiple sites across the mammalian brain. *Nat Methods* **13**, 325–328 (2016).
27. Stamatakis AM, Schachter MJ, Gulati S, Zitelli KT, Malanowski S et al. Simultaneous optogenetics and cellular resolution calcium imaging during active behavior using a miniaturized microscope. *Front Neurosci* **12**, 496 (2018).
28. Yang WJ, Carrillo-Reid L, Bando Y, Peterka DS, Yuste R. Simultaneous two-photon imaging and two-photon optogenetics of cortical circuits in three dimensions. *eLife* **7**, e32671 (2018).
29. Falkner AL, Grosenick L, Davidson TJ, Deisseroth K, Lin DY. Hypothalamic control of male aggression-seeking behavior. *Nat Neurosci* **19**, 596–604 (2016).
30. Wan YQ, Wang MQ, Zhang SR, Xie BB. Availability and safety assessment of infrared neural stimulation at high repetition rate through an implantable optrode. *J Innovative Opt Health Sci* **14**, 2150014 (2021).
31. Chen TW, Wardill TJ, Sun Y, Pulver SR, Renninger SL et al. Ultrasensitive fluorescent proteins for imaging neuronal activity. *Nature* **499**, 295–300 (2013).
32. Dana H, Mohar B, Sun Y, Narayan S, Gordus A et al. Sensitive red protein calcium indicators for imaging neural activity. *eLife* **5**, e12727 (2016).
33. Sun FM, Zeng JZ, Jing M, Zhou JH, Feng JS et al. A genetically encoded fluorescent sensor enables rapid and specific detection of dopamine in flies, fish, and mice. *Cell* **174**, 481–496.e19 (2018).
34. Patriarchi T, Mohebi A, Sun JQ, Marley A, Liang RQ et al. An expanded palette of dopamine sensors for multiplex imaging in vivo. *Nat Methods* **17**, 1147–1155 (2020).
35. Luo F, Wei Y, Wang ZY, Luo MM, Hu J. Genetically encoded neural activity indicators. *Brain Sci Adv* **4**, 1–15 (2018).
36. Helmchen F, Denk W. Deep tissue two-photon microscopy. *Nat Methods* **2**, 932–940 (2005).
37. Barretto RPJ, Messerschmidt B, Schnitzer MJ. *In vivo* fluorescence imaging with high-resolution microlenses. *Nat Methods* **6**, 511–512 (2009).
38. Bocarsly ME, Jiang WC, Wang C, Dudman JT, Ji N et al. Minimally invasive microendoscopy system for in vivo functional imaging of deep nuclei in the mouse brain. *Biomed Opt Express* **6**,

4546–4556 (2015).
39. Resendez SL, Jennings JH, Ung RL, Namboodiri VMK, Zhou ZC et al. Visualization of cortical, subcortical and deep brain neural circuit dynamics during naturalistic mammalian behavior with head-mounted microscopes and chronically implanted lenses. *Nat Protoc* **11**, 566–597 (2016).
40. Qin H, Lu J, Jin WJ, Chen XW, Fu L. Multichannel fiber photometry for mapping axonal terminal activity in a restricted brain region in freely moving mice. *Neurophotonics* **6**, 035011 (2019).
41. Sych Y, Chernysheva M, Sumanovski LT, Helmchen F. High-density multi-fiber photometry for studying large-scale brain circuit dynamics. *Nat Methods* **16**, 553–560 (2019).
42. Pisano F, Pisanello M, Lee SJ, Lee J, Maglie E et al. Depth-resolved fiber photometry with a single tapered optical fiber implant. *Nat Methods* **16**, 1185–1192 (2019).
43. Klapoetke NC, Murata Y, Kim SS, Pulver SR, Birdsey-Benson A et al. Independent optical excitation of distinct neural populations. *Nat Methods* **11**, 338–346 (2014).
44. Coda S, Thompson AJ, Kennedy GT, Roche KL, Ayaru L et al. Fluorescence lifetime spectroscopy of tissue autofluorescence in normal and diseased colon measured *ex vivo* using a fiber-optic probe. *Biomed Opt Express* **5**, 515–538 (2014).
45. Zhang L, Pan J, Zhang Z, Wu H, Yao N et al. Ultrasensitive skin-like wearable optical sensors based on glass micro/nanofibers. *Opto-Electron Adv* **3**, 190022 (2020).
46. Tan FZ, Lyu W, Chen SY, Liu ZY, Yu CY. Contactless vital signs monitoring based on few-mode and multi-core fibers. *Opto-Electron Adv* **3**, 190034 (2020).
47. Simone K, Füzesi T, Rosenegger D, Bains J, Murari K. Open-source, cost-effective system for low-light *in vivo* fiber photometry. *Neurophotonics* **5**, 025006 (2018).
48. Gunaydin LA, Grosenick L, Finkelstein JC, Kauvar IV, Fenno LE et al. Natural neural projection dynamics underlying social behavior. *Cell* **157**, 1535–1551 (2014).
49. Lerner TN, Shilyansky C, Davidson TJ, Evans KE, Beier KT et al. Intact-brain analyses reveal distinct information carried by SNc dopamine subcircuits. *Cell* **162**, 635–647 (2015).
50. Owen SF, Kreitzer AC. An open-source control system for *in vivo* fluorescence measurements from deep-brain structures. *J Neurosci Methods* **311**, 170–177 (2019).
51. Bromberg-Martin ES, Matsumoto M, Hikosaka O. Dopamine in motivational control: rewarding, aversive, and alerting. *Neuron* **68**, 815–834 (2010).
52. Björklund A, Dunnett SB. Dopamine neuron systems in the brain: an update. *Trends Neurosci* **30**, 194–202 (2007).
53. Yuan L, Dou YN, Sun YG. Topography of reward and aversion encoding in the mesolimbic dopaminergic system. *J Neurosci* **39**, 6472–6481 (2019).
54. Peng WL, Wu ZF, Song K, Zhang SY, Li YL et al. Regulation of sleep homeostasis mediator adenosine by basal forebrain glutamatergic neurons. *Science* **369**, eabb0556 (2020).
55. Nieh EH, Vander Weele CM, Matthews GA, Presbrey KN, Wichmann R et al. Inhibitory input from the lateral hypothalamus to the ventral tegmental area disinhibits dopamine neurons and promotes behavioral activation. *Neuron* **90**, 1286–1298 (2016).
56. Schultz W. Dopamine reward prediction-error signalling: a two-component response. *Nat Rev Neurosci* **17**, 183–195 (2016).
57. Covey DP, Cheer JF. Accumbal dopamine release tracks the expectation of dopamine neuron-mediated reinforcement. *Cell Rep* **27**, 481–490.e3 (2019).
58. Dreyer JK, Herrik KF, Berg RW, Hounsgaard JD. Influence of phasic and tonic dopamine release on receptor activation. *J Neurosci* **30**, 14273–14283 (2010).
59. Kim CK, Sanchez MI, Hoerbelt P, Fenno LE, Malenka RC et al. A molecular calcium integrator reveals a striatal cell type driving aversion. *Cell* **183**, 2003–2019.e16 (2020).
60. Yao SQ, Yuan P, Ouellette B, Zhou T, Mortrud M et al. RecV recombinase system for in vivo targeted optogenomic modifications of single cells or cell populations. *Nat Methods* **17**, 422–429 (2020).
61. Lin JY, Knutsen PM, Muller A, Kleinfeld D, Tsien RY. ReaChR: a red-shifted variant of channelrhodopsin enables deep transcranial optogenetic excitation. *Nat Neurosci* **16**, 1499–1508 (2013).

Acknowledgements

We thank J. Snyder for commenting and editing the manuscript, all the members in Minmin Luo lab, Ling Fu lab, and Jingfeng Zhou for their insightful comments, Youtong zhou and Dr. Fei Zhao (Chinese institute for brain research) for the AAV-hSyn-EGFP-RPL10 virus, Dr. Yulong Li (Peking University) for the pAAV-hSyn-GRAB$_{DA2m}$ plasmid. Minmin Luo is supported by Beijing Municipal Government. Ling Fu is supported by the National Natural Science Foundation of China (Grant Nos. 61890952) and the Director Fund of WNLO. We also thank the Optical Bioimaging Core Facility of WNLO-HUST and the Analytical and Testing Center of HUST for data acquisition.

Author contributions

Q. C. Guo, L. Fu, and M. M. Luo proposed the original idea and supervised the project. Q. C. Guo, S. Wang, M. Y. Jia, X. W. Gao designed the optical system. Q. C. Guo and Z. Y. Qi performed the experiments. Q. C. Guo and Z. Y. Qi discussed the results and co-wrote the paper. All authors commented on the manuscript.

Competing interests

The authors declare no competing financial interests.

Ethical statement

All experiments were approved and were conducted in accordance with the guidelines of the committee on animal health and care of the National Institute of Biological Sciences (NIBS), Beijing.

Supplementary information

Supplementary information for this paper is available at
https://doi.org/10.29026/oea.2022.210081